Latency characteristics of the short-wavelength-sensitive cones and their associated pathways

R. J. Lee   Department of Psychology, Durham University, UK

J. D. Mollon   Department of Experimental Psychology, University of Cambridge, UK

Q. Zaidi   Graduate Program in Vision Science, SUNY College of Optometry, New York, USA

H. E. Smithson   Department of Psychology, Durham University, UK

There are many distinct types of retinal ganglion and LGN cells that have opponent cone inputs and which may carry chromatic information. Of interest are the asymmetries in those LGN cells that carry S-cone signals: in S-ON cells, S+ signals are opposed by (L + M) whereas, in many S-OFF cells, L+ signals are opposed by (S + M), giving $-S + L - M$ (C. Tailby, S. G. Solomon, & P. Lennie, 2008). However, the S-opponent pathway is traditionally modeled as $\pm[S - (L + M)]$. A phase lag of the S-cone signal has been inferred from psychophysical thresholds for discriminating combinations of simultaneous sinusoidal modulations along $\pm[L - M]$ and $\pm[S - (L + M)]$ directions (C. F. Stromeyer, R. T. Eskew, R. E. Kronauer, & L. Spillmann, 1991). We extend this experiment, measuring discrimination thresholds as a function of the phase delay between pairs of orthogonal component modulations. When one of the components isolates the tritan axis, there are phase delays at which discrimination is impossible; when neither component is aligned with the tritan axis, discrimination is possible at all delays. The data imply that the S-cone signal is delayed by approximately 12 ms relative to (L − M) responses. Given that post-receptoral mechanisms show diverse tuning around the tritan axis, we suggest that the delay arises before the S-opponent channels are constructed, possibly in the S-cones themselves.

Keywords: color vision, temporal vision, S-cones, retinal ganglion cells, lateral geniculate nucleus, latency, phase lags

Introduction

Are the signals of the short-wavelength sensitive (S-) cones delayed in their transmission to a central site where perceptual decisions are made? If so, where does the delay arise? These issues gain fresh interest from the discovery that there is a plurality of chromatically opponent pathways that carry signals originating in the S-cones.

To investigate the delays in the S-cone pathway, we measured thresholds for discriminating stimuli that offered different temporal modulations to the three cone classes, using a method introduced by Stromeyer, Eskew, Kronauer, and Spillmann (1991). In our experiments, the stimulus was modulated concurrently along two axes of color space. In one condition, these axes were the cardinal axes identified by Krauskopf, Williams, and Heeley (1982) and in the other they were intermediate to the cardinal axes. In one interval of a two-alternative temporal forced-choice (2ATFC) trial, the two modulations were in a phase relationship of θ and in the other interval they were in the relationship $\theta - \pi$. The observer's task was to distinguish these phase relationships. When $\theta = \pi/2$, the stimuli can always be distinguished—whether the axes are cardinal or intermediate. However, in the case of the cardinal axes, and not the intermediate axes, it is possible to introduce a phase advance that renders the two stimuli indistinguishable. We use this result to estimate the delay of the S-cone signal and to consider the site at which the delay arises.

Early chromatic pathways

To extract chromatic information, signals from photoreceptors with different spectral sensitivities must be compared. These comparisons begin in the neural circuitry of the retina, and recent work has revealed fresh details of these circuits (e.g., Dacey & Packer, 2003). The number and diversity of cells that perform color opponent comparisons are greater than previously thought.

The biological substrate of the color mechanism that compares signals from the long- and middle-wavelength sensitive (L- and M-) cones is generally accepted to be the ON and OFF-midget ganglion cells (but see Calkins & Sterling, 1999; Rodieck, 1991). The midget ganglion cells receive opposed L and M input and project to parvocellular

layers of the lateral geniculate nucleus (LGN; Wiesel & Hubel, 1966). For the S-opponent chromatic pathway, the S-ON signal has for several years been identified with the small bistratified ganglion cell, which draws excitatory inputs from S-cones and inhibitory inputs from L- and M-cones (Dacey & Lee, 1994). However, in the retina, the S-OFF pathway has been difficult to identify and remains controversial (Klug, Herr, Ngo, Sterling, & Schein, 2003; Lee, Telkes, & Grünert, 2005). The recent discovery of several additional, low-density, LGN-projecting ganglion cells has identified a possible substrate for the S-OFF signal and has additionally revealed further chromatically opponent S-ON ganglion cells. In brief summary, these are the intrinsically photosensitive, melanopsin-containing ganglion cells, which have an S-OFF opponent receptive field (Dacey et al., 2005), the large sparse monostratified ganglion cells (S-OFF), and large sparse bistratified ganglion cells (S-ON; Dacey, Peterson, & Robinson, 2002).

In the LGN, cells with S-OFF responses have been found reliably for many years. Valberg, Lee, and Tigwell (1986) report that the L-cone input to such cells, if present, is synergistic with the S-cone input, and opposed to an excitatory M-cone input. In contrast, Tailby, Solomon, and Lennie (2008) report that the S-OFF signal most commonly has the same sign as the M-cone signal and is opposed by L-signals. In other S-OFF cells, the S-signal is antagonistic to both L- and M-signals. Thus it appears that there is some heterogeneity in the chromatic tuning of the S-OFF population.

The separability of pathways that respond to S-increments and S-decrements has also been demonstrated psychophysically (Krauskopf & Zaidi, 1986; Shinomori, Spillmann, & Werner, 1999). The inferred S-ON and S-OFF pathways additionally show several asymmetries: They differ in the ratio of L- to M-inputs (McLellan & Eskew, 2000) and in spatial summation areas (Vassilev, Mihaylova, Racheva, Zlatkova, & Anderson, 2003).

Delay of the S-cone signal

Schnapf, Nunn, Meister, and Baylor (1990) made direct measurements of the temporal response of Macaque photoreceptors. Only three S-cones were studied in detail, but their kinetics and sensitivities were roughly comparable to those of the L- and M-cones. Using silent substitution, Yeh, Lee, and Kremers (1995) measured the temporal characteristics of signals of the three cone types at the ganglion cell level. They found similar temporal modulation transfer functions for +L − M, +M − L, and +S − (L + M) cells, for both excitatory and inhibitory cone inputs.

Tailby et al. (2008) measured the temporal frequency selectivity of S+ and S− LGN cells that were driven either by S-cone isolating modulation or by achromatic modulation. The peak sensitivity for both cell types was around 3 Hz when driven by S-cone isolating modulation, but around 7 Hz when driven by achromatic modulation. They argue therefore that the poor temporal resolution of the S-cone pathways arises early in the retina. However, they find no evidence for an accompanying *phase delay* of the S-cone signal, relative to the L- and M-cone signals provided by parvocellular cells.

So, perhaps the S-cone delay arises only after the LGN. In support of this, Cottaris and De Valois (1998), recording from cortical area V1 in the Macaque, found that S-opponent signals were available only after 96–135 ms, whereas L/M-opponent signals were available after 68–95 ms. They additionally found that cells with late S-cone inputs dynamically change their chromatic tuning over time, which they suggest implies that the S-cone signal is amplified and delayed in V1 before being combined with L/M-opponent signals.

Consistent with the suggestion that S-cone signals arrive late at a central site, several authors have found longer reaction times to S-cone chromatic signals than to L- and M-cone chromatic signals (McKeefry, Parry, & Murray, 2003; Smithson & Mollon, 2004). Analysis of visual evoked potentials (VEPs) also suggests a relative delay of the S-cone signal (Rabin, Switkes, Crognale, Schneck, & Adams, 1994; Robson & Kulikowski, 1998). These studies all find a latency difference, but they differ in their estimates of the magnitude of that difference. Furthermore the relative delay can be different for manual, saccadic, or perceptual responses (Bompas & Sumner, 2008), indicating that delays are injected after the divergence of the pathways that support these different tasks.

Psychophysical measurement of the temporal impulse response functions (IRFs) reveals a slower time course for S-cone signals than for luminance signals. Consistent with the physiological differences in S-ON and S-OFF pathways, the IRF for S-cone increments and decrements differs, with faster responses to increments (Shinomori & Werner, 2008).

The Peake effect

Our experiment exploits a phenomenon first described by Miss Olive E. Peake (Hartridge, 1949), and which we refer to as the Peake effect. A rapidly presented sequence of hues appears noticeably different when the sequence is ordered in a clockwise (CW) sense around the hue circle (decreasing dominant wavelengths), compared to the reverse counterclockwise (CCW) sense. The flickering sequence appears to contain different predominant colors depending on the direction of procession. CW stimuli typically appear orange and sky blue, while CCW stimuli typically appear lime and magenta. The effect was later described by Davidoff, Aspinall, and Hill (1978) and Hill, Rodger, and Smalridge (1980). These authors constructed their stimuli by CW or CCW rotation of tubes or discs colored with brightness-matched colored papers.

The rapid rates of presentation required for the Peake effect (approximately seven to twelve cycles around the hue circle per second) far exceed the rates at which temporal order judgments can be made. So, the Peake effect is counterintuitive in that we might expect stimuli that differ only in the order in which the hues are presented, and not in the loci of hues themselves, to be indistinguishable. During the transmission of the neural response associated with CW and CCW stimuli to the point at which the perceptual comparison can be made, the signals must become distorted, such that the locus of hues visited is different for the two senses of modulation. It is possible to imagine several classes of mechanism through which such distortions might be introduced—for example, asymmetries in temporal masking between opponent mechanisms that are unequally distributed around the hue circle (Spillmann, 1990; Spillmann & Neumeyer, 1984), or differential latencies between color mechanisms, possibly at a stage as early as the cones (Hill et al., 1980). In support of the latter suggestion, Stromeyer et al. (1991) found that introducing a phase advance to the modulation of the S-cones was sufficient to null this latency, rendering the CW and CCW stimuli indiscriminable. Models of the Peake effect that rely instead on asymmetric tuning of mechanisms around the hue circle predict that no such null is possible. Furthermore, Stromeyer et al.'s result is consistent with separate evidence that the signal originating in the S-cones is delayed at some stage during transmission to a central site (see above).

The ability to counteract the Peake effect by adjusting only the phase of an S-cone isolating modulation implies that there is a neural delay, and that it is associated with a mechanism that is aligned with the tritan axis. This result is particularly interesting in the light of the growing evidence summarized above that suggests that the S-opponent mechanism is not characterized by a symmetric bipolar pathway and that there are post-receptoral channels not aligned with the cardinal axes of Krauskopf et al. (1982).

We start by replicating Stromeyer et al.'s (1991) experiment, with component modulations that are aligned to the cardinal axes, and check the null. Secondly we extend the experiment to use component modulations that are oriented intermediate to the cardinal axes. The lights that comprise a hue-circle locus can be constructed from component modulations along any pair of orthogonal axes. However, when the component modulations are intermediate to the cardinal axes, we predict that no null should be possible, since we now cannot introduce a phase advance that is confined to the short-wave pathway.

Predictions

To introduce formally the present experiments, and to make specific predictions, we first describe the geometric properties of the chromatic loci that comprise our stimuli.

Temporal modulation around a circular locus in the equiluminant plane of DKL color space (Derrington, Krauskopf, & Lennie, 1984) can be thought of as the sum of two component modulations along two orthogonal directions, temporally offset by a phase difference of $\pi/2$ radians.

First consider component modulations that are aligned to the cardinal axes. When the tritan modulation *leads* the $\pm[L - M]$ modulation by $\pi/2$ (or lags by $3\pi/2$) the sense of procession is CW; whereas when the tritan modulation *lags* by $\pi/2$ the sense of procession is CCW. Figure 1 illustrates these relationships. The $\pm[L - M]$ modulation is represented by a thin black line. The solid blue line represents the phase-advanced tritan modulation (and CW procession around the hue circle) and the solid red line represents the phase-delayed tritan modulation (and the CCW procession around the hue circle). Inverting one of the component modulations (by introducing a phase difference of π or, equivalently, by multiplying the sinusoid by -1) reverses the direction of procession.

The dashed lines represent additional phase shifts (φ) of the S-cone signal, to simulate neural delays in the S-cone pathway. When combined with the $\pm[L - M]$ modulation the resultant chromatic loci are no longer circular. In the CW case, the phase difference between the component modulations becomes $\pi/2 + \varphi$, and the chromatic locus is an ellipse oriented along the positive diagonal in DKL space. In the CCW case, the phase difference becomes $-\pi/2 + \varphi$, and the elliptical locus is oriented along the negative diagonal. (The orientation of the ellipses is determined by the relative magnitudes of the component modulations; in a space in which the excursions are balanced, the ellipses are oriented at 45°.) The elliptical loci in Figure 1 provide a plausible explanation of the Peake effect (Stromeyer et al., 1991). The stimuli appear to flicker between the dominant hues at the extremes of the major axes of the elliptical loci: Between orange and sky blue for CW stimuli, and between lime and magenta for CCW stimuli. At the rates of presentation required for the effect, a neural delay of a few tens of milliseconds produces ellipses with the lengths of major and minor axes in the ratio 2:1.

If the response to tritan modulation is delayed, it should be possible to find a physical advance of the tritan modulation that nulls the neural delay, causing the resultant chromatic loci to become circular once more. Figure 2A shows the combined effects of putative neural delays of the S-cone response (φ) and physical phase differences between component modulations (θ). The blue and red lines in each plot represent the chromatic loci generated by combining chromatic modulations with phase differences of $\theta - \varphi$ and $\theta - \varphi - \pi$, respectively, which correspond to CW and CCW processions. The top row in Figure 2A represents zero neural delay of the S-cone response and is a description of the physical stimuli. Subsequent rows represent neural phase delays (φ) of 0.1π, 0.2π, and 0.3π. The successive plots from left to right in
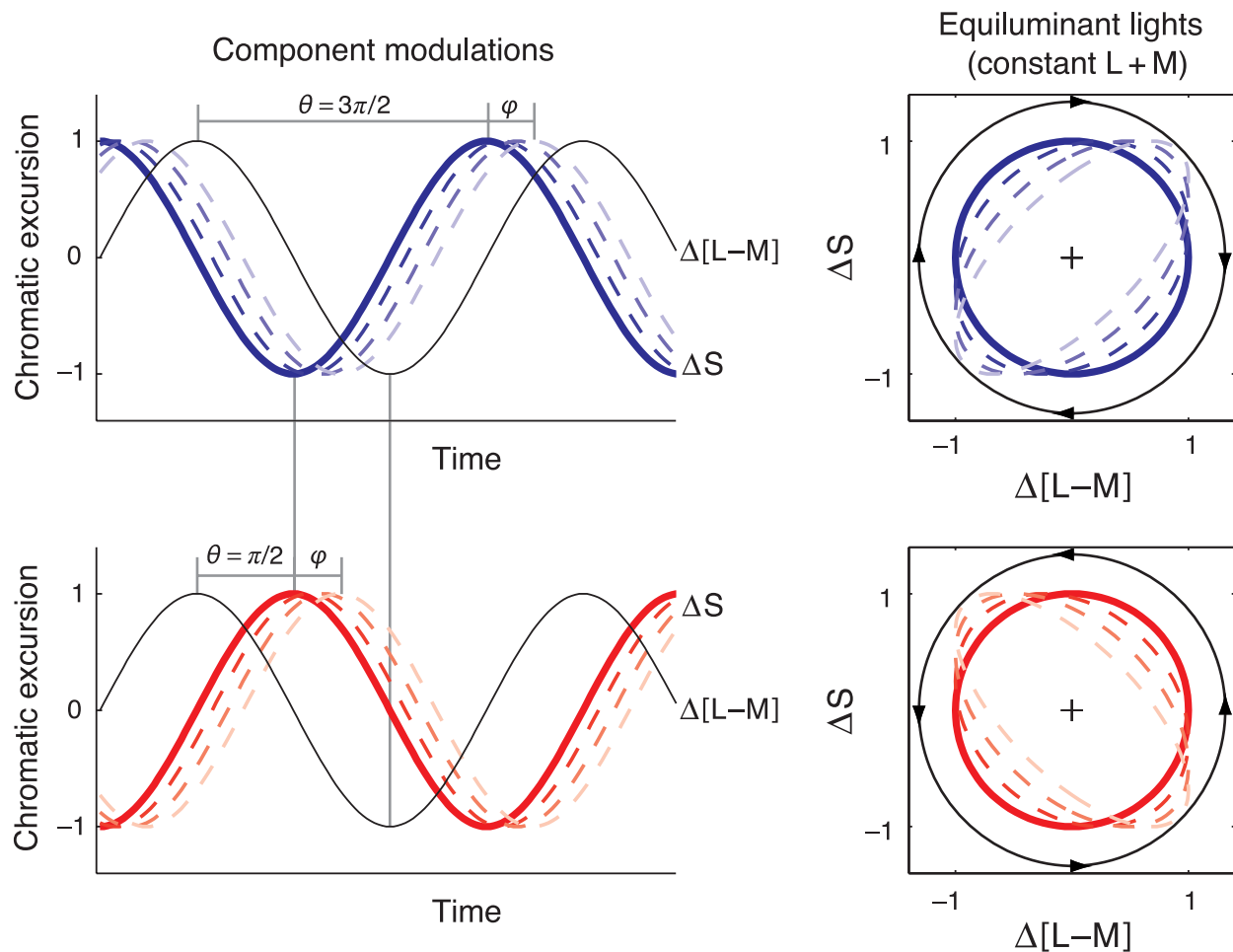
Figure 1. The sequences of chromaticities produced by sinusoidal Δ[L − M] and ΔS modulations in different phase relationships. The plots on the left show modulations as a function of time; the plots on the right show the loci of chromaticities that are visited. In the plots on the left, the Δ[L − M] signal is used as a reference (thin black solid line). When this is combined with a ΔS modulation with a $3\pi/2$ phase shift (top-left panel, thick blue solid line), the resulting sequence of chromaticities follows a circular clockwise (CW) trajectory in the equiluminant plane of DKL color space (top-right plot, thick blue solid line). If the ΔS modulation has a phase of $\pi/2$ relative to the Δ[L − M] signal (lower left panel, thick red solid line), the sequence of chromaticities plots out a circular counterclockwise (CCW) trajectory (bottom-right panel, thick red solid line). If the phase of the ΔS modulation is delayed from $3\pi/2$ (dashed curves in upper panels), then the chromaticities follow elliptical trajectories in color space. These ellipses are oriented with their major axis along the positive diagonal, becoming more eccentric with larger phase differences, up to a phase difference of π. For delays from $\pi/2$ (dashed curves in lower panels), the ellipses are oriented with their major axis along the negative diagonal. Importantly, inverting the S-cone modulation by introducing a phase difference of π reverses the sense of procession and the orientation of the ellipse (and defines the difference between upper and lower panels).

each row indicate loci that are generated from component modulations with physical phase differences (θ) of 0 to π, in steps of 0.1π. In each row, the plot outlined in orange corresponds to resultant phase differences of $\pm\pi/2$ (i.e., $(\theta - \varphi) = \pm\pi/2$), where CW and CCW loci overlap. In the extreme cases when the resultant signals are perfectly in phase or in counter-phase (i.e., $(\theta - \varphi) = 0$ or $(\theta - \varphi) = \pi$) the loci collapse to straight lines along the positive and negative diagonals. In these cases the "CW" and "CCW" loci are maximally discriminable.

The panels of Figure 2A provide illustrations of the family of chromatic loci used by Stromeyer et al. (1991)

to measure the latency of the S-cone response. By measuring discriminability of CW and CCW loci as a function of the phase delay between component modulations they were able to find a minimum of discriminability from which they inferred the neural phase delay.

When component modulations are along axes that are intermediate to the cardinal axes (our "intermediate axes" condition), the stimulus loci are effectively rotated in DKL space. These loci are represented in the top row of Figure 2B. A phase difference of $\theta = \pi/2$ or $\theta = 3\pi/2$ again results in a stimulus that changes chromaticity in time around a circular locus, and the corresponding plot is
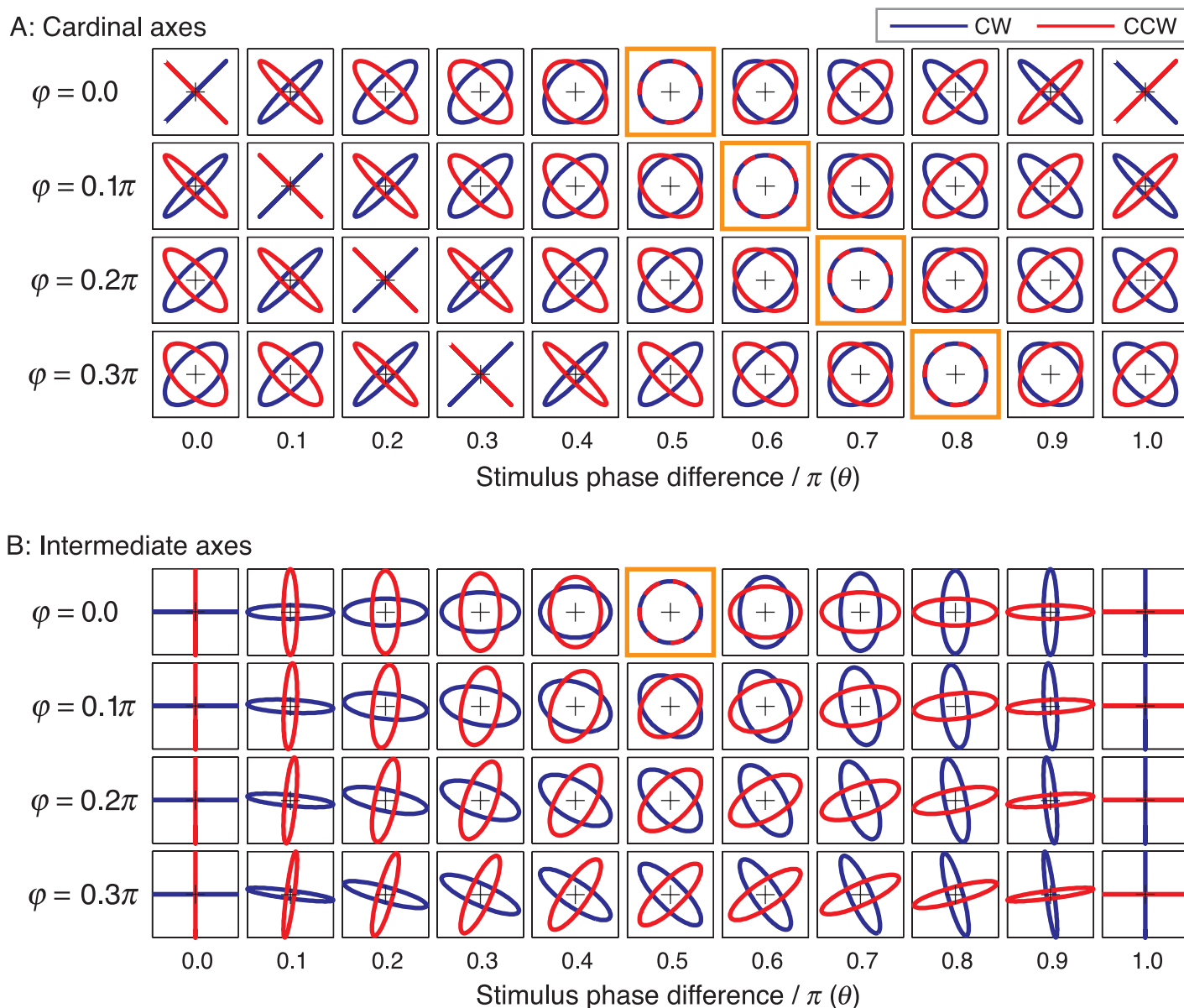
Figure 2. Simulated chromatic loci reaching a central site when the stimuli are composed of sinusoidal modulations (upper panel, A) along the cardinal directions of color space or (bottom panel, B) along our intermediate axes. Each square represents the equiluminant plane of DKL color space. CW stimulus loci (where the component modulations have a phase difference of θ) are shown in blue, and CCW loci (where the component modulations have a phase difference of $\theta - \pi$) are shown in red. Each column of plots represents a different value of θ and each row represents a different simulated neural phase shift φ introduced by the S-cones or the putative $\pm[S - (L + M)]$ mechanism. Note how, in the cardinal axes condition, increasing φ translates the pattern of ellipses to the right but in the intermediate axes condition, increasing φ rotates the ellipses and the patterns remain symmetrical around $\theta = 0.5\pi$.

outlined in orange. For phase differences other than $3\pi/2$ and $\pi/2$, the stimulus loci are elliptical, but now the major axes align with the cardinal axes, and in the extreme cases when $\theta = 0$ and $\theta = \pi$, the locus collapses to a straight line along one or other cardinal axis. The subsequent rows of Figure 2B indicate the distorted loci that result from phase shifts of the S-cone response (φ) of 0.1π, 0.2π, and 0.3π. In contrast to the cardinal axis plots shown in Figure 2A, there is now no stimulus phase difference (θ) at which the CW and CCW loci overlap. The maximally discriminable

loci are in all cases at phase differences of $\theta = 0$ or $\theta = \pi$. Here the CW and CCW loci are aligned with the cardinal axes and stimuli would appear as flickering exchanges between cherry and teal or between violet and chartreuse. As the phase differences approach $\theta = \pm\pi/2$, CW and CCW loci become more similar, with the most similar occurring at $\theta = \pm\pi/2$. The similarity at $\theta = \pm\pi/2$ depends upon the simulated phase shift of the S-cone response (φ): Loci overlap when $\varphi = 0$ and are progressively dissimilar as φ increases.

In our experiment, in addition to measuring the discriminability of CW and CCW loci constructed from phase-shifted modulations along the cardinal axes, we test loci constructed from phase-shifted modulations along the intermediate axes.

Methods

Our methods follow those of Stromeyer et al. (1991). Throughout the investigation we sought to measure the threshold amplitude for discriminating between CW and CCW stimuli as a function of the phase difference (θ) between component modulations. We used a two-alternative temporal forced-choice (2ATFC) task. One interval contained stimuli processing in a CW sense, and consisting of component modulations with a phase difference of θ. The other interval contained stimuli processing in a CCW sense, with a phase difference of $\theta - \pi$. The order of the stimuli was chosen at random, with equal likelihood of CW followed by CCW or vice versa.

During an experimental session, the amplitude of one component modulation was adjusted until the observer could no longer discriminate CW and CCW processions. Initial modulation amplitudes were made as large as possible within the color space gamut of our apparatus while maintaining perceptually equated amplitudes for both components (see below). At these amplitudes either component alone was well above detection threshold. Therefore, by adjusting only one modulation at a time, we guaranteed that the CW and CCW modulations were always suprathreshold, even when their discriminability was at threshold.

There were several reasons why we adopted this approach, rather than requiring observers to manipulate θ in order to find a point at which discrimination was impossible: (i) the task becomes one of objective performance rather than phenomenal judgment, (ii) the variation of threshold with θ allows us to estimate the null point from the entire data set, (iii) we are able to test the full curve against a quantitative model, (iv) in the case of the intermediate axes, there proves to be no null point.

Apparatus

All stimuli were generated with a computer-controlled four-primary Maxwellian view optical system (Pokorny, Smithson, & Quinlan, 2004). This apparatus was configured to present chromatic stimuli in a center–surround spatial configuration. The circular center field subtended 2° of visual angle, and the annular surround subtended 8°. Stimuli were viewed monocularly through an artificial pupil of 3-mm diameter. The observer's head was held stationary with a bite bar.

The center and surround fields were generated independently by mixing two sets of four LEDs behind interference filters that provided a narrow-band output. The primaries had peak outputs at 459 nm (blue), 516 nm (cyan), 561 nm (green), and 664 nm (red). The relation between the intensities specified by the program and those produced by the diodes was established with a radiometer (UDT Instruments, Orlando, FL). A linearizing look-up table was then created to generate a mapping from the level requested in software to the luminance output of each LED.

Since four primaries were mixed, we were able to specify the relative stimulations of four photoreceptor types—the three classes of cone and the rods. A transformation matrix was used to convert between desired photoreceptor excitations and outputs of the primaries.

The transformation matrix was derived from the cone sensitivity functions (Stockman & Sharpe, 2000; Stockman, Sharpe, & Fach, 1999), the sensitivity function of the rods ($V'(\lambda)$), and spectral measurements of the primaries, measured with a telescopic spectroradiometer (Gamma Scientific, San Diego, CA). The L- and M-cone fundamentals were scaled so that L + M = $V*(\lambda)$, the photopic luminosity function appropriate for the Stockman and Sharpe standard observer fundamentals (Sharpe, Stockman, Jagla, & Jägle, 2005), itself normalized to peak at unity. The S-cone fundamental was scaled so that S/(L + M) = 1.0 for the point on the spectrum locus that corresponds to the maximum S-cone stimulation (MacLeod & Boynton, 1979).

Calibration for individual observers

The relative scalings of the photoreceptor sensitivity functions were further adjusted to account for individual differences, using the color matching technique described by Pokorny et al. (2004). In this procedure, the observer makes chromatic matches between a mixture of the red and cyan primaries and a mixture of the green and blue primaries. The relative outputs of each of the center primaries after matching were compared to the matching values for the standard observer and used to scale the standard sensitivities to the primary lights. This procedure should correct for individual differences in photopigment sensitivities and macular pigment and lens density (Shapiro, Pokorny, & Smith, 1996). The scaling for each individual observer allows us to produce luminance-equated stimuli. To minimize the contrast at the border between the central and surround fields, each of the surround LEDs in turn was perceptually matched in brightness to the center LED having the same wavelength composition.

The intermediate axes modulations were intended to create balanced stimulation along S-opponent and L/M-opponent directions in color space. Since modulation in one channel does not have an intrinsically equivalent

magnitude in the other channel, there is no accepted method of achieving this scaling. We chose to equate the perceived saturation of colors at different angles in color space around equal energy white (EEW). We presented a 1-Hz modulation around the hue circle and allowed the observer to adjust the relative amplitudes of the component modulations such that the number of perceived hues was maximized. The procedure was repeated for CW and CCW processions, and the optimal scaling was taken to be the average of four settings for each direction. A scaling factor of L/(L + M): S/(L + M) = 1.14:1 was appropriate for both observers.

A mismatch in the scaling of stimuli in the S-opponent and L/M-opponent directions in color space is not predicted (according to the model outlined below) to change the critical phase delay in the cardinal axes condition, nor the phase delay at which discrimination is easiest in the intermediate axes condition.

Stimulus characteristics

The nominal luminance of the time-averaged stimulus (for both center and surround fields) was approximately 20 cd m^{-2}, and the time-averaged cone signals were those that would be elicited in the Stockman and Sharpe observer by an EEW spectrum. In a version of the MacLeod–Boynton chromaticity diagram that was constructed from these cone sensitivities, the mean chromaticity coordinates were [L/(L + M), S/(L + M)] = [0.6652, 0.0194].

Using the four-primary colorimeter we were able to hold constant the summed L- and M-cone stimulation to maintain the modulations in the equiluminant plane, and simultaneously to hold rod stimulation constant, while generating chromatic modulations.

The surround field was held steady in order to maintain uniform adaptation over an extended area of retina so that even small lapses of fixation would not have caused the test stimulus to fall on a nonadapted region. Test stimuli comprised temporal modulations of the center field, generated by combining two sinusoidal temporal modulations along orthogonal directions in the equiluminant plane. The extreme points visited had chromaticity coordinates L/(L + M)$_{max}$ = 0.6777; L/(L + M)$_{min}$ = 0.6527 and S/(L + M)$_{max}$ = 0.0304; S/(L + M)$_{min}$ = 0.0084.

To simplify description, we use the convention introduced by Derrington et al. (DKL, 1984) in which the origin of the space corresponds to the white point. Our space is modified from that of DKL only in that it is constructed from the cone sensitivities of Stockman and Sharpe. Thus, in this space, sinusoidal modulations in $\Delta[L - M]$ and ΔS had amplitudes of $1.14 \times 2a$ and a, respectively, where a set the amplitude of the modulations and was 0.0110 in our experiment.

The temporal frequency of the sinusoidal modulations was 10 Hz. Note that one cycle of the component modulations corresponds to one complete procession around the elliptical locus. Each stimulus lasted 1356 ms (13.56 cycles), including 339 ms at the beginning and end during which the modulation depth of the flickering stimulus was ramped on or off with a raised cosinusoidal envelope. The temporal phase of the stimulus was randomized relative to the envelope on every presentation.

We use (i) component chromatic modulations that are aligned with the cardinal axes of the equiluminant plane (i.e., $\Delta[S - (L + M)]$, which simplifies to ΔS since L + M is held constant, and $\Delta[L - M]$), and (ii) component modulations that are oriented intermediate to the cardinal axes (i.e., $\Delta[S + L - M]$ and $\Delta[S - L + M]$). The component modulations had a relative phase difference of θ ("CW") or $\theta - \pi$ ("CCW").

Experimental procedure

The observers' task was a 2AFTC in which they had to select the interval that contained the stimulus with a θ phase difference, responding by pressing one of two buttons—each button corresponding to one of the intervals. Since the stimuli with a θ phase difference were not associated with a consistent appearance across stimulus conditions, it was necessary to give observers the opportunity to learn which of the combinations they should be reporting. Feedback was given immediately in the form of a tone of high or low pitch.

After two practice trials, a staircase reduced the amplitude of one of the component modulations. We estimated the 71%-correct point on the psychometric function using a two-down-one-up staircase procedure, which reduced the amplitude of one component after two correct responses and increased it after one incorrect response, in logarithmic steps. The staircase progressed according to observers' performance in reliably identifying the correct stimulus, and we did not restrict the cues on which the observer was allowed to base his decision, although in most cases both observers reported that they were using the difference in predominant hues. Each staircase terminated after eight reversals, and we geometrically averaged the final six of these to estimate the threshold amplitude of the adjusted component modulation for this value of θ. Two independent staircases, with identical stimulus starting parameters, were interleaved in each run.

Experimental conditions

In each run we measured amplitude thresholds at a particular value of θ, to obtain threshold as a function of θ, from 0 to 1.2π. Measurements for different values of θ were run in a counterbalanced order. For each value of θ in each condition, we obtained at least two pairs of staircase estimates of threshold. In separate conditions we adjusted

one or other of the component modulations. We ran counterbalanced sets of measurements for component modulations that were along cardinal axes and for component modulations that were along intermediate axes. So in total we obtained threshold as a function of θ for four combinations of stimulus conditions: (i) $\Delta[L - M]$ and ΔS, adjust ΔS; (ii) $\Delta[L - M]$ and ΔS, adjust $\Delta[L - M]$; (iii) $\Delta[S+ L - M]$ and $\Delta[S - L + M]$, adjust $\Delta[S - L + M]$; (iv) $\Delta[S + L - M]$ and $\Delta[S - L + M]$, adjust $\Delta[S + L - M]$.

Two observers, both authors, completed all conditions. They both had normal color vision and corrected-to-normal acuity.

Results

Figure 3 shows the complete data set for our study. Thresholds for discriminating between the two processions are plotted against the phase difference between component modulations, for all four stimulus conditions for both observers. Panels A, B, E, and F show data for the cardinal axes condition, panels C, D, G, and G show data for the intermediate axes condition. Panels A and E show data obtained by reducing the amplitude of the ΔS modulation. Panels B and F show data obtained by reducing the amplitude of the $\Delta[L - M]$ modulation. Panels C and G show data obtained by reducing the amplitude of the $\Delta[S - L + M]$ modulation. Panels D and H show data obtained by reducing the amplitude of the $\Delta[S + L - M]$ modulation. In each panel, the ordinate represents the amplitude of the staircase-adjusted modulation, relative to the fixed-amplitude modulation, at threshold. So values of 1.0 indicate equal modulation amplitudes, in DKL color space, for the two component modulations. Symbols show the geometric mean of at least two pairs of staircase endpoints. Error bars show one geometric standard deviation above and below the geometric mean. Smooth curves through the data points show predictions of the model described below.

"Cardinal" axes

For both observers in the cardinal axes conditions, thresholds were strongly dependent on θ, the physical phase difference between component modulations. There were some phase differences at which it was not possible to make a threshold measurement, since the task was impossible at the maximum modulation amplitudes in gamut. Thresholds that we were unable to measure are marked as red arrows along the top edge of the plots, at the appropriate value of θ. Thresholds that we were able to measure on some occasions but not others are marked with orange arrows. In both cases these should be taken as

underestimates of threshold. For both observers, the peak values occurred at values of θ around 0.75π. In comparing panels A vs. B and E vs. F, it is also clear that changing which of the component modulations was adjusted by the staircase does not affect the pattern of thresholds.

"Intermediate" axes

Data for the intermediate axes conditions are shown in Figures 3C, 3D, 3G, and 3H. The format of these plots is the same as for the cardinal axes conditions, but now the physical phase difference θ is the difference between the component modulations along our intermediate axes. Thresholds show some dependence on θ, but in the intermediate axes condition there was no value of θ for which the task became impossible. The highest thresholds were always close to $\theta = 0.5\pi$, and not as far from $\theta = 0.5\pi$ as the locations of the peaks in the cardinal axis case.

Models

Model description

The Lissajous figures presented in Figure 2 are constructed by considering the way in which CW and CCW loci would be distorted by a phase shift of the S-cone response. Here we derive a model to predict our measured discrimination thresholds as a function of the physical phase delay between component modulations. Our predictions are based on first estimating the signals presented to a central site for CW and CCW processions (represented schematically by the red and blue lines in Figure 2, assuming different delays of the S-cone response in successive rows) and then deriving a decision variable from the difference between signals for CW and CCW modulations.

Here, we make an explicit link between discrimination threshold and the similarity of predicted CW and CCW loci. A simple metric is to calculate the Weber contrast between the maximum excursion of the CW stimulus and the minimum excursion of the CCW stimulus, both measured as Euclidian distances from the time-averaged chromaticity in the equiluminant plane of DKL color space, and to use the inverse of this contrast to predict thresholds. Similar templates are obtained by calculating the root-mean-square radial difference between CW and CCW loci. In their gross features, these templates resemble that used by Stromeyer et al. (1991) based on the form $|\cos(\theta - \varphi)|^{-1}$.

The derivation of the model is summarized in Appendix. The most important parameter in the model is the phase
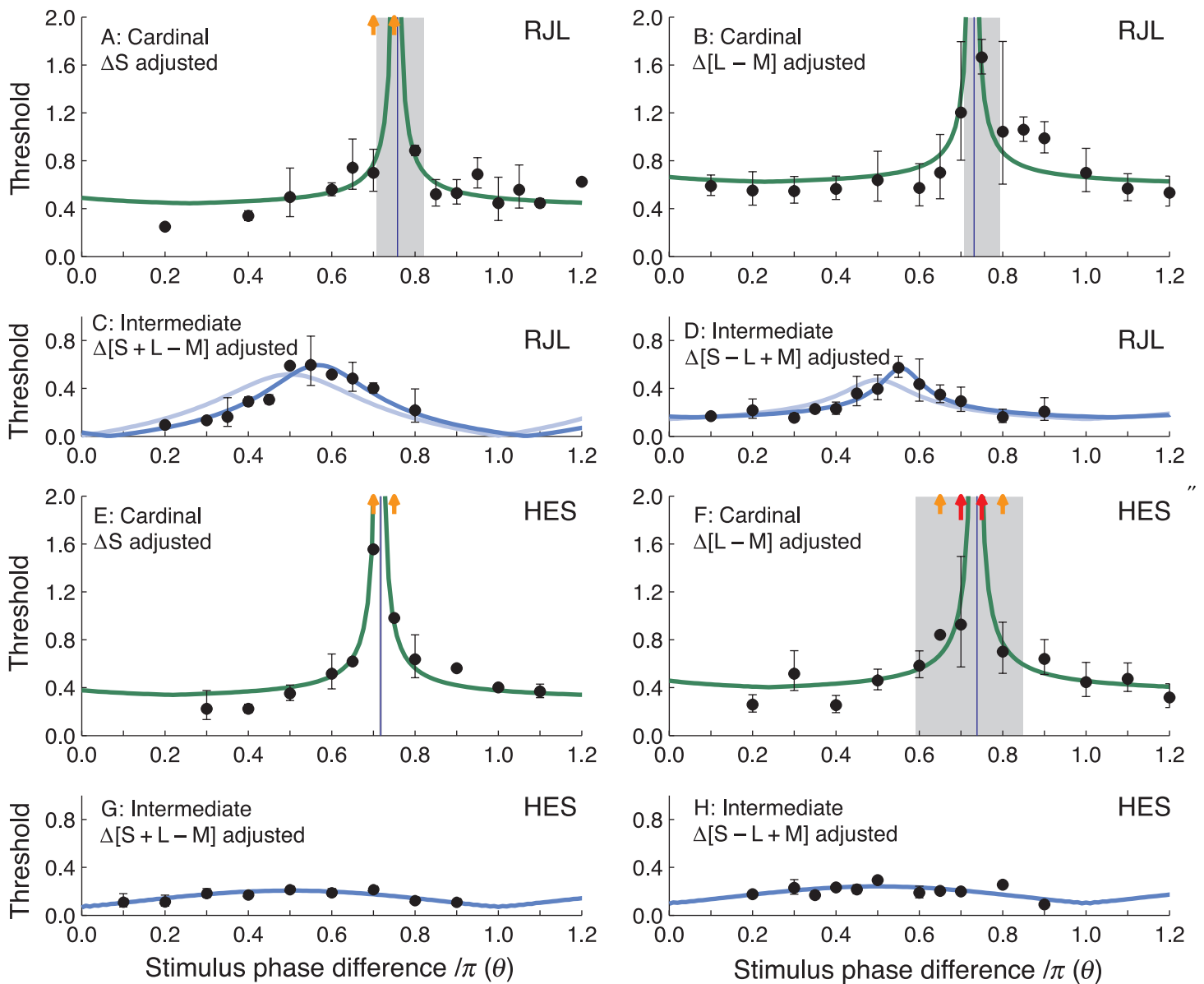
Figure 3. Measured thresholds for discriminating CW and CCW processions, as a function of θ, the phase difference between component modulations. Panels A–D represent results from observer RJL and panels E–H are for observer HES. Panels A, B, E, and F show data from the experimental conditions when component modulations were along the cardinal axes. Panels C, D, G, and H show data from conditions in which component modulations were along intermediate axes. The left-hand column of panels represents conditions in which the ΔS modulation or the $\Delta[S + L - M]$ modulation was adjusted by the staircase. The right-hand column of panels represents conditions in which the $\Delta[L - M]$ modulation or the $\Delta[S - L + M]$ modulation was adjusted by the staircase. Data points are the geometric mean of at least four staircases. Error bars indicate one geometric standard deviation above and below the geometric mean of several staircase results. Arrows along the top edges of each panel indicate that we failed to measure thresholds at the corresponding phase difference on some attempts (small orange arrows) or on all attempts (large red arrows). The green and blue lines represent predictions of the model described in the text and shown in Figure 4, with parameters adjusted to obtain least-squares best fits to the data. The faint lines in panels C and D represent the simple version of the intermediate axes model in which the rotation of the axes is fixed, and darker blue lines represent the model in which the axis rotation can vary. The gray shaded areas represent the range of values of θ at which the peaks of the predicted thresholds may occur, based on a 95% confidence interval on the neural phase delay variable.

shift of the S-cone response and varying this produces the family of templates presented in Figure 4. To fit these templates to our data, we also include vertical offset and scaling.

If there were no phase delays, discrimination thresholds would tend to infinity at $\theta = \pi/2$ and would show the same pattern for the cardinal axes and intermediate axes conditions. If the phase delay (φ) between mechanisms

aligned to the cardinal axes were nonzero, thresholds in the cardinal axis case would tend to infinity when $(\theta - \varphi) = \pi/2$. The location of the peak would therefore identify the phase delay. In the intermediate axes condition the peak threshold would be at $\theta = \pi/2$, irrespective of the neural phase delay. For a nonzero phase delay, discrimination

would be possible at all values of θ, and thresholds would not tend to infinity.

Model fits

The smooth curves in Figure 3 show the results of a least-squares fit to the data obtained in each condition (see Table A1 for best fitting values of the three free parameters: neural phase lag (φ) between the putative underlying mechanisms; vertical scale factor; and vertical offset). For both observers, the fit parameters are similar after adjusting either axis in the staircase. We tested this statistically using an F test to compare the difference between the total sum-squared residuals of fits to the data from each condition and the sum-squared residuals of a fit to the pooled data from both conditions combined, and found no evidence to suggest a difference.
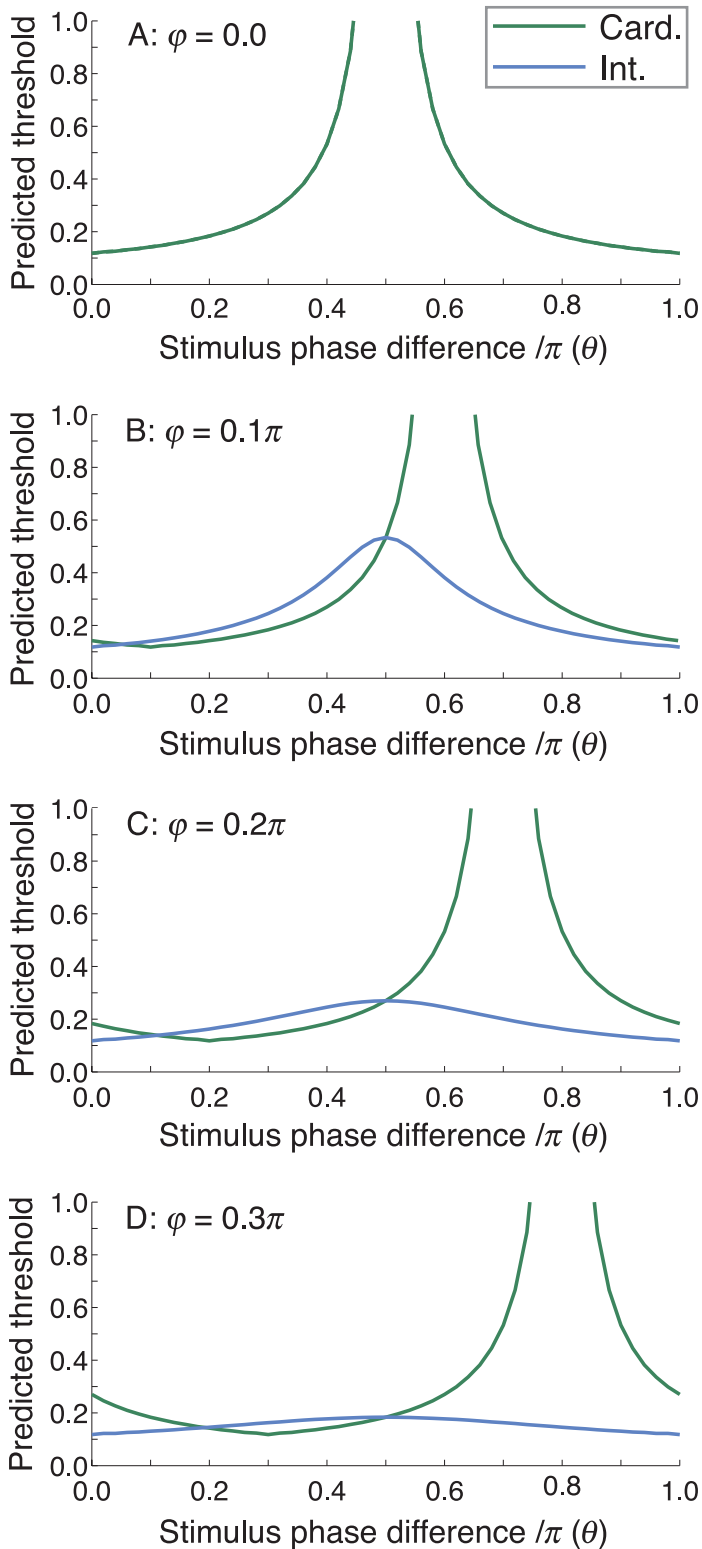
Cardinal axes conditions

Smooth green lines in panels A, B, E, and F show fits for the cardinal axes conditions. In terms of neural mechanisms, the phase lag parameter is the most interesting. It is determined by the position on the abscissa at which thresholds peak. For a neural phase lag $\varphi = 0$ the peak occurs at $\theta = 0.5\pi$, and in general the peak occurs at $\theta = 0.5\pi + \varphi$. To obtain 95% confidence limits on this parameter we stepped through a range of φ values and found the limits within which the other two parameters could be adjusted to obtain fits not statistically different from the original, optimal one.

Importantly, the confidence limits on the neural phase lag parameter indicate that it was significantly different from zero, and therefore that the S-cone pathway is significantly delayed relative to the L vs. M pathway. Averaging the estimates obtained from the condition in which $\Delta[L - M]$ was adjusted and those obtained when ΔS was adjusted, gives values of $\varphi = 0.25\pi$ and $\varphi = 0.23\pi$ for observers RJL and HES, respectively. At the modulation frequency of 10 Hz, this corresponds to a neural delay, of the S-cone pathway relative to the L vs. M pathway, of between 10.1 ms and 16.1 ms for the two observers.

Figure 4. Predicted thresholds for discriminating between a stimulus in which component sinusoidal modulations have a phase difference of θ and a stimulus in which the phase difference is $\theta - \pi$, as a function of θ. Green lines show predictions when component modulations aligned with the cardinal axes, and blue lines show predictions for the intermediate axes. The uppermost panel assumes no neural delay between the response to ΔS and $\Delta[L - M]$, and each subsequent panel shows predictions for successive small increases in the phase delay of the ΔS response, denoted by φ.

There are some subtle features of the data that are not well captured by the simple model. For example, in the cardinal axes condition, thresholds on the left-hand side of the peak are lower than thresholds on the right-hand side of the peak. This occurs for both observers, irrespective of whether we adjust the S or L/M modulation amplitude. The model predicts that thresholds are symmetric about the maximum threshold, as can be seen from the Lissajous figures (Figure 2) and from the template curves (Figure 4). Systematic differences between the data and the model suggest that there are measurable asymmetries in the thresholds. We consider a possible source of these asymmetries in the Discussion section.

Intermediate axes conditions

Smooth faint blue lines in panels C, D, G, and H show fits for the intermediate axes conditions. The neural delay is assumed to be between ΔS and $[L - M]$, but the model now considers component modulations that are angled 45° to the cardinal axes in our color space, so the physical delay cannot directly null the neural delay. This model can account for the main properties of our data and has the same three free parameters as before: neural phase lag (φ); vertical scale factor; and vertical offset. Best fitting parameters are provided in Table A1. For the intermediate axes condition the neural phase lag parameter is not well constrained by the data, since once the delay is greater than zero its effects are similar to the effect of the vertical scale factor. Upper confidence limits cannot be obtained for this parameter, but lower confidence limits confirm that the delay is not zero.

In this form, the model for the intermediate axis condition is rigid in that the location of the peak is constrained to be at $\theta = 0.5\pi$. The data, particularly for observer RJL, however, show systematic deviations from this, with the maximum thresholds obtained slightly above $\theta = 0.5\pi$. A simple explanation of this discrepancy is that, in the intermediate axes condition, the two component modulations may not be perfectly matched in their effect on the opponent mechanisms. For example, one component might produce relatively more excitation in the S-opponent mechanism than the other. By allowing an additional parameter to vary in the model, namely the rotation of the intermediate axes relative to the cardinal axes (previously fixed at 45°), the model can account for the slight adjustment of the peak away from $\theta = 0.5\pi$. The rotations required to give the best fit for the data, for observer RJL and for each of the adjusted modulations, are 32° (ΔS adjusted) and 21° ($\Delta[L - M]$ adjusted). These fits are shown with heavy lines in Figures 3C and 3D. The extra variation accounted for by the additional parameter significantly reduces the overall variation, as determined by comparing the sum-of-squared deviations of the data in the two models with an F test. Systematic deviations (i.e., an over-estimation of thresholds on the left shoulder of the peak, and an under-estimation of thresholds on the right of

the peak) are improved by the extra parameter. For observer HES the additional free parameter did not significantly improve the fits. Again, best fitting parameters are included in Table A1.

Discussion

Do S-cone signal delays explain the Peake effect?

A simple model that assumes a phase shift of the S-cone response provides a good fit to the data sets, for both the cardinal and intermediate axes conditions. Thresholds in cardinal axes conditions tend to infinity at $\theta = 0.5\pi + \varphi$, whereas CW and CCW stimuli are discriminable at all phase delays between the intermediate component modulations.

In the cardinal axes condition, the equiluminant S-opponent modulation is a pure tritan stimulus—it modulates only the S-cones. If there were a delay only in the response of the S-cones themselves, the physical phase delay we introduce to the modulated lights would cancel the delay in the cones, and hence the input to all subsequent pathways. For the peak thresholds in the cardinal axis condition to be shifted from $\pi/2$, we assume that the delay must be apparent at the point at which the responses to the component modulations are combined to solve the perceptual task. Therefore, if the neural delay arises in the S-cones, we additionally infer that it must be propagated through the system, implying that the S-cone signal must remain confined to pathways that maintain a delay relative to the L/M-opponent signal.

Mechanisms later in the S-cone signal pathway may also contribute to the apparent delay of the S-cone signals revealed in our perceptual task. If these mechanisms are aligned with the tritan axis, as $\pm[S - (L + M)]$, delays in receptoral and post-receptoral stages simply add. The locations of the peaks in the cardinal axes data identify the combined delay, and there is no way in this experiment to tease apart the two sources.

However, if the chromatic tuning of these later mechanisms is not aligned with the tritan axis, delays injected here would be predicted to distort the CW and CCW loci, generating signals that might support discrimination of the CW and CCW stimuli at all values of θ. Since CW and CCW loci in the cardinal axes conditions became indiscriminable at critical values of θ, we found no evidence that delayed responses from nontritan-aligned mechanisms were reliably available to observers in our psychophysical task. Indeed, if opponent mechanisms show a diversity of tuning around the tritan axis, and if these mechanisms contribute to performance in our task, then the neural delay that we null must be at a pre-opponent stage.

The purpose of our intermediate axes condition was to use component modulations that are unlikely to be aligned with the neural mechanisms that exhibit relative delays. As predicted, loci for the intermediate axis condition remained sufficiently distinct at all physical phase delays to support good discrimination.

Comparison to Stromeyer et al. (1991)

For the case of modulations on the cardinal axes, our replication yields the same pattern of thresholds as was found by Stromeyer et al. (1991). There were some differences between our experimental conditions and those of Stromeyer et al. However, our use of cone-isolating modulations and maintenance of rod excitation at a constant level did not change the results, supporting the conclusion that cone mechanisms were successfully isolated in the original study. A potentially more interesting difference is the surround adaptation in the two experiments: Our test stimulus had a time-averaged chromaticity of white and was surrounded by a white annular field; Stromeyer et al.'s test field time-averaged to white, but their surround had a yellow-green appearance. However, we do not see any gross differences between the results obtained in the two cases. Our replication therefore suggests that the original results were not dependent on the biased surround adaptation.

Stromeyer et al. (1991) proposed that differences in the appearance of CW and CCW processions around a hue circle stem from a phase delay of the S-cone signal. From their discrimination data they estimated that the S signal lagged the L/M opponent signal by about 0.41π–0.50π at 10 Hz (a latency of about 21–25 ms). Our estimates of the phase delay of the S-cone signal from the cardinal axes condition are lower, with mean best-fitting values of 11 and 12 ms for the two observers. Adaptation state critically determines the temporal response of visual mechanisms (e.g., Stockman, Langendorfer, Smithson, & Sharpe, 2006), with faster responses obtained at higher adaptation levels. The S-cone quantal catch for the stimuli used by Stromeyer et al. was higher than ours (by approximately one log unit), but the adapting chromaticity was similar, such that the relative adaptation states of color mechanisms were approximately equivalent in the two studies.

Critically, the interpretation of the Peake effect in terms of a delay of the S-cone signal is further supported by the results in our intermediate axes condition. If there were no significant relative delays, discrimination of CW and CCW stimuli would be predicted to be impossible when loci were physically overlapping. This is not the case, and CW and CCW stimuli are discriminable at all phase delays between the intermediate component modulations. Model fits to our results confirm that the required value of the phase-delay parameter is significantly greater than zero.

Comparison to other estimates of the magnitude of the S-cone signal delay

There has long been interest in determining the relative latencies of the cone signals. Physiological studies remain inconclusive: Some authors (e.g., Schnapf et al., 1990; Yeh et al., 1995) argue for similar temporal resolutions at early stages while other authors (e.g., Tailby et al., 2008) suggest that the poor temporal resolution of the S-cone pathway arises early in the retina. However, few studies have reported phase delays explicitly and Tailby et al. at least show a dissociation between phase delay and temporal resolution.

In psychophysical studies the question is complicated by the potential involvement of multiple post-receptoral pathways. At the simplest level, residual luminance transients in the test stimuli can support rapid responses (Mollon, 1980), effectively hiding differences between stimuli intended to isolate chromatic pathways (Ueno, Pokorny, & Smith, 1985). Even equiluminant exchanges in L- and M-cone excitations can elicit responses in parasol ganglion cells (Lee, Martin, & Valberg, 1989), which might support performance in psychophysical tasks. Interestingly, this parasol cell response is not elicited by stimuli that isolate the S-cones, so S-cone stimuli might be at a disadvantage in a behavioral task that compares equiluminant S-cone and L/M cone exchanges. Chatterjee and Callaway (2002) claim a small (10%) but consistent S-cone input to magnocellular neurons in Macaque LGN. However, Sun, Smithson, Zaidi, and Lee (2006a, 2006b) find no significant S-cone input to magnocellular and parvocellular ganglion cells, at least under neutral adaptation. Using dynamic luminance noise to isolate chromatic channels, and using similar chromatic adaptation conditions to ours, Smithson and Mollon (2004) found that reaction times to liminal S-opponent and L/M-opponent stimuli showed mean differences of 13, 6, and 12 ms for their three observers. Other groups have found larger differences, of 40 ms or more (McKeefry et al., 2003), with similarly equated stimuli but without luminance noise.

Interestingly, Stromeyer et al. (1991) compared the results for their main discrimination task (in which one component modulation was S-isolating and the other was an equiluminant L $-$ M exchange) with results obtained when an S-isolating modulation was paired with a luminance (L + M) modulation. This revealed a further delay of S-cone signals in the inferred luminance pathway of 28 ms, consistent with other reports that delayed S-cone signals feed into luminance pathways (Lee & Stromeyer, 1989; Stockman, MacLeod, & DePriest, 1987). They additionally used conditions in which observers were able to switch their criterion from a chromatic judgment to an achromatic judgment and again they found a dissociation between phase delays estimated for inferred chromatic and luminance pathways.

When comparing across photoreceptors with different spectral sensitivities it is essential to specify their relative adaptation states. Furthermore, perceptual latency depends on signal strength, with stronger stimuli eliciting more rapid responses (Mollon & Krauskopf, 1973; Piéron, 1931). Paying particular attention to these two factors, Blake, Land, and Mollon (2008) have demonstrated that when the S-cones are given a "fair" chance (i.e., the S-cone adaptation state is equated to the L- and M-cone adaptation states such that the thresholds for both are equivalently elevated above absolute threshold, and excursions of equal discriminability are used), there is negligible delay in the phase of a moving S-cone stimulus relative to a long-wave stimulus. The contrasts of our component modulations were matched in units of discrimination threshold, but the equal-energy time-averaged adaptation placed the S-cones in a relatively more adapted state than the adaptation used by Blake et al. (2008). More adapted receptors are predicted to have shorter latencies so this difference in relative adaptation is unable to account for the relative delay we measured.

Given that the absolute response latency depends on adaptation state, it is interesting to determine the way in which relative latencies vary with adaptation level for different latency estimates. Irrespective of whether the S-cone delay was assessed against a chromatic modulation or against a luminance modulation, Stromeyer et al. (1991) found that a one log unit increase in the adapting level of the S-cones decreased the S-cone delay by 17 ms. The relative adaptation state of the S-cones did not change the *difference* between the S-cone delay relative to the inferred luminance pathway and the S-cone delay relative to the inferred chromatic pathway. A parsimonious explanation of this result is that the adaptation introduces latency differences early in the visual pathway, probably in the S-cones themselves.

Alternative models

The gross characteristics of CW and CCW discriminations in the cardinal axes conditions—namely that we reliably find that a simple advance of the tritan modulation is sufficient to render CW and CCW loci indiscriminable—are well captured by assuming a delay in a tritan aligned mechanism. However, as noted above, there are small systematic differences between our data and the model. In particular, the model cannot account for asymmetries in thresholds around the peak.

Our model assumes bipolar opponent mechanisms, where the tuning of ON and OFF sub-mechanisms is co-linear in DKL space. To account for the asymmetries in our data, we might appeal to additional cone opponent mechanisms that may not be aligned to the cardinal axes. Contributions from such mechanisms, perhaps with their own phase delays, have the potential to distort CW and CCW loci differently for phase advances and phase delays relative to the null, thus causing asymmetric thresholds around the peak.

Several authors have suggested that color mechanisms might be more accurately described as unipolar mechanisms, with rectified outputs, rather than bipolar mechanisms (e.g., Chen, Foley, & Brainard, 2000; Krauskopf et al., 1982). For the S-opponent system the mechanisms that respond to increments and decrements have been shown to be separable (Shinomori et al., 1999), and to respond with different latencies (Shinomori & Werner, 2008). Given that different classes of cell respond to opposite directions along the same axis of color space, we must also acknowledge that responses of any mechanism may be nonlinear, and that these nonlinearities may differ between cells responding to chromatic changes in different directions (e.g., Giulianini & Eskew, 2007; Zaidi & Shapiro, 1993).

It is notoriously difficult to decide how best to model the combination of signals from different mechanisms. Indeed, there has been a long debate about this issue for the combination of information from the cardinal mechanisms (see Eskew, 2009 for review). In the model that we fit to our data, the signal reaching central sites is the vector sum of modulations along the $\Delta[L - M]$ and $\Delta[S - (L + M)]$ axes. One way to extend the model to incorporate a chromatic mechanism with a preferred direction intermediate to the cardinal axes (e.g., the S-OFF LGN cells characterized by Tailby et al., 2008) is to assume inputs from rectified independent mechanisms ($+L - M$; $-L + M$; $+S - L - M$; and $-S + L - M$). Another scheme would be to first combine multiply-tuned opponent cell signals to generate only two color opponent dimensions, and then treat these as orthogonal axes of a 2D chromaticity space, as in the classical model.

These complications present a vast array of possible models, each with many unknown parameters. Detailed prediction of psychophysical thresholds is impossible from such modeling. Instead, we concentrate on correspondence between qualitative features of the data and models, namely the existence, location, and symmetry of peaks in threshold as a function of phase difference between component modulations.

On the one hand, the slight asymmetries in our data indicate the involvement of mechanisms more complex than those captured by our simple model. However, given that we find substantial failures of discrimination in the cardinal axes condition, it is likely that the neural delay arises in mechanisms tuned to the tritan axes, and not in a family of mechanisms with diverse tuning. The simplest explanation is that delays are injected at the receptor level, but injection at a unitary tritan-aligned, post-receptoral mechanism cannot be ruled out. The results of the discrimination experiment imply that the delay of the S-cone signal propagates through the visual system to at least the neural locus at which responses to the component modulations are combined. It is an open question whether later

stages are perceptually calibrated to represent physical simultaneity of events in the world.

Summary

Every model we have considered predicts that, if there are no relative delays in the pathways supporting the discrimination of CW and CCW stimuli, we should see large peaks at $\pi/2$ and $3\pi/2$, in both the cardinal and intermediate axes conditions. We confirm Stromeyer et al.'s (1991) finding that the peaks are displaced from these locations for the cardinal axes condition and further show that peaks are much reduced in the intermediate axes condition, a result that similarly is consistent with there being significant neural delays.

Given that post-receptoral mechanisms show a diversity of tuning around the tritan axis, and assuming these mechanisms contribute to performance in this task, we suggest that strong peaks in the cardinal axis data are not consistent with delays injected at a post-receptoral site. The source of the delay is therefore likely to be before the S-opponent mechanisms are constructed, possibly in the S-cones themselves. Alternatively, if the delay does arise late in the pathway, then our results suggest that the only channels contributing to the task are ones aligned with the cardinal axes of color space.

Appendix

Model equations

The equation predicting discrimination threshold in our model takes the following general form:

$$T = \left(\frac{\max(r_{CW})}{\min(r_{CCW})} - 1 \right)^{-1}, \tag{A1}$$

where T is proportional to threshold and r_{CW} and r_{CCW} are functions describing the radii of the CW and CCW ellipses, respectively:

$$r_{CW} = \left(\begin{array}{c} (\sin(t)\cos(\alpha) - \sin(t-\theta)\sin(\alpha))^2 + \\ (\sin(t+\varphi)\sin(\alpha) + \sin(t-\theta+\varphi)\cos(\alpha))^2 \end{array} \right)^{\frac{1}{2}}, \tag{A2}$$

$$r_{CCW} = \left(\begin{array}{c} (\sin(t)\cos(\alpha) - \sin(t-\theta-\pi)\sin(\alpha))^2 + \\ (\sin(t+\varphi)\sin(\alpha) + \sin(t-\theta+\varphi-\pi)\cos(\alpha))^2 \end{array} \right)^{\frac{1}{2}}, \tag{A3}$$

where α is the rotation of the stimulus component axes relative to the cardinal ones, θ is the phase difference between the two components, φ is a phase delay introduced by the S-cones or any tritan-aligned mechanism, and t is a parameter such that $0 < t < 2\pi$.

In the cardinal axes condition, these equations simplify to

$$r_{CW} = \left(\sin^2 t + \sin^2(t-\theta+\varphi) \right)^{\frac{1}{2}}, \tag{A4}$$

$$r_{CCW} = \left(\sin^2 t + \sin^2(t-\theta+\varphi-\pi) \right)^{\frac{1}{2}}, \tag{A5}$$

and the minima and maxima can be found by taking the derivatives

$$\frac{dr_{CW}}{dt} = \left(\sin^2 t + \sin^2(t-\theta+\varphi) \right)^{-\frac{1}{2}} \times (\sin t \cos t + \sin(t-\theta+\varphi)\cos(t-\theta+\varphi)), \tag{A6}$$

$$\frac{dr_{CCW}}{dt} = \left(\sin^2 t + \sin^2(t-\theta+\varphi-\pi) \right)^{-\frac{1}{2}} \times (\sin t \cos t + \sin(t-\theta+\varphi-\pi)\cos(t-\theta+\varphi-\pi)). \tag{A7}$$

The minima and maxima of the radius functions occur when

$$t = \frac{\theta-\varphi}{2} + \left(k + \frac{1}{2} \right)\pi, \tag{A8}$$

or

$$t = \frac{\theta-\varphi}{2} + k\pi, \tag{A9}$$

where k is an integer $k \in \mathbb{Z}$.

Substituting these into above gives

$$T = \left(\frac{\left(\sin^2\left(\frac{\theta-\varphi+(2k+1)\pi}{2} \right) + \sin^2\left(\frac{\varphi-\theta+(2k+1)\pi}{2} \right) \right)^{\frac{1}{2}}}{\left(\sin^2\left(\frac{\theta-\varphi+(2k+2)\pi}{2} \right) + \sin^2\left(\frac{\varphi-\theta+2k\pi}{2} \right) \right)^{\frac{1}{2}}} - 1 \right)^{-1}, \tag{A10}$$

Observer	Adjusted modulation	Cardinal axes		Intermediate axes, fixed rotation		Intermediate axes, free rotation	
		ΔS	$\Delta L - M$	$\Delta S + L - M$	$\Delta S - L + M$	$\Delta S + L - M$	$\Delta S - L + M$
RJL	$S - (L + M)$	0.258	0.231	0.169	0.085	0.140	0.075
	phase delay/π	$(0.208 < \varphi < 0.322)$	$(0.208 < \varphi < 0.294)$	$(0.033 < \varphi)$	$(0.031 < \varphi)$	$(0.075 < \varphi)$	$(0.049 < \varphi)$
	$S - (L + M)$	12.9	11.6	8.5	4.3	7.0	3.7
	time delay (ms)	$(10.4 < t < 16.1)$	$(10.4 < t < 14.7)$	$(1.7 < t)$	$(1.5 < t)$	$(3.7 < t)$	$(2.4 < t)$
	Vertical scale factor	0.062	0.064	0.383	0.102	0.290	0.069
	Vertical offset	0.445	0.624	0.005	0.144	0.001	0.158
	Axis angle (°)			45	45	31.4	20.6
	RMS error	0.095	0.113	0.100	0.061	0.041	0.022
HES	$S - (L + M)$	0.218	0.239	0.419	0.385	0.416	0.384
	phase delay/π	$(0.214 < \varphi < 0.221)$	$(0.201 < \varphi < 0.279)$	$(0.043 < \varphi)$	$(0.013 < \varphi)$	$(0.047 < \varphi)$	$(0.020 < \varphi)$
	$S - (L + M)$	10.9	11.9	20.9	19.235	20.8	19.2
	time delay (ms)	$(10.7 < t < 11.0)$	$(10.1 < t < 13.9)$	$(2.2 < t)$	$(0.7 < t)$	$(2.3 < t)$	$(1.0 < t)$
	Vertical scale factor	0.070	0.085	0.955	0.644	0.949	0.669
	Vertical offset	0.339	0.403	0.065	0.096	0.061	0.091
	Axis angle (°)			45	45	44.5	44.5
	RMS error	0.065	0.089	0.018	0.038	0.017	0.037

Table A1. A summary of the parameters of the models fitted to data across all experimental conditions.

for $0 < (\theta - \varphi) < \frac{\pi}{2}$ and $\frac{3\pi}{2} < (\theta - \varphi) < \pi$ and

$$T = \left(\frac{\left(\sin^2\left(\frac{\theta - \varphi + 2k\pi}{2}\right) + \sin^2\left(\frac{\varphi - \theta + 2k\pi}{2}\right) \right)^{\frac{1}{2}}}{\left(\sin^2\left(\frac{\theta - \varphi + 3k\pi}{2}\right) + \sin^2\left(\frac{\varphi - \theta + (2k-1)\pi}{2}\right) \right)^{\frac{1}{2}}} - 1 \right)^{-1},$$

(A11)

for $\frac{\pi}{2} < (\theta - \varphi) < \frac{3\pi}{2}$.

In the intermediate axes condition, the derivatives of the radius functions do not simplify, leaving equations that are difficult to solve. Our templates for the intermediate axes were generated numerically.

Model fit parameters

Table A1.

References

Blake, Z., Land, T., & Mollon, J. (2008). Relative latencies of cone signals measured by a moving vernier task. *Journal of Vision, 8*(16):16, 1–11, doi:10.1167/8.16.16, http://journalofvision.org/8/16/16/. [PubMed] [Article]

Bompas, A., & Sumner, P. (2008). Sensory sluggishness dissociates saccadic, manual, and perceptual responses: An S-cone study. *Journal of Vision, 8*(8):10, 1–13, doi:10.1167/8.8.10, http://journalofvision.org/8/8/10/. [PubMed] [Article]

Calkins, D. J., & Sterling, P. (1999). Evidence that circuits for spatial and color vision segregate at the first retinal synapse. *Neuron, 24,* 313–321. [PubMed]

Chatterjee, S., & Callaway, E. M. (2002). S cone contributions to the magnocellular visual pathway in macaque monkey. *Neuron, 35,* 1135–1146. [PubMed]

Chen, C. C., Foley, J. M., & Brainard, D. H. (2000). Detection of chromoluminance patterns on chromoluminance pedestals II: Model. *Vision Research, 40,* 789–803. [PubMed]

Cottaris, N. P., & De Valois, R. L. (1998). Temporal dynamics of chromatic tuning in macaque primary visual cortex. *Nature, 395,* 896–900. [PubMed]

Dacey, D. M., & Lee, B. B. (1994). The 'blue-on' opponent pathway in primate retina originates from a distinct bistratified ganglion-cell type. *Nature, 367,* 731–735. [PubMed]

Dacey, D. M., Liao, H. W., Peterson, B. B., Robinson, F. R., Smith, V. C., Pokorny, J., et al. (2005). Melanopsin-expressing ganglion cells in primate retina signal colour and irradiance and project to the LGN. *Nature, 433,* 749–754. [PubMed]

Dacey, D. M., & Packer, O. S. (2003). Colour coding in the primate retina: Diverse cell types and cone-specific circuitry. *Current Opinion in Neurobiology, 13,* 421–427. [PubMed]

Dacey, D. M., Peterson, B. B., & Robinson, F. R. (2002). Identification of an S-cone opponent OFF pathway in the macaque monkey retina: Morphology, physiology and possible circuitry. *Investigative Ophthalmology & Visual Science, 43,* U840–U840.

Davidoff, J. B., Aspinall, P. A., & Hill, A. R. (1978). A new colour flicker phenomenon. *Modern Problems in Ophthalmology, 19,* 187–188. [PubMed]

Derrington, A. M., Krauskopf, J., & Lennie, P. (1984). Chromatic mechanisms in lateral geniculate nucleus of macaque. *The Journal of Physiology, 357,* 241–265. [PubMed] [Article]

Eskew, R. T., Jr. (2009). Higher order color mechanisms: A critical review. *Vision Research, 49,* 2686–2704. [PubMed]

Giulianini, F., & Eskew, R. T. (2007). Theory of chromatic noise masking applied to testing linearity of S-cone detection mechanisms. *Journal of the Optical Society of America A, Optics, Image Science, and Vision, 24,* 2604–2621. [PubMed]

Hartridge, H. (1949). *Colours and how we see them.* London: Bell.

Hill, A. R., Rodger, G., & Smalridge, L. (1980). Some further observations on the colour flicker phenomenon. In G. Verriest (Ed.), *Colour vision deficiencies V* (pp. 381–384). Bristol, UK: Adam Hilger.

Klug, K., Herr, S., Ngo, I. T., Sterling, P., & Schein, S. (2003). Macaque retina contains an S-cone OFF midget pathway. *Journal of Neuroscience, 23,* 9881–9887. [PubMed] [Article]

Krauskopf, J., Williams, D. R., & Heeley, D. W. (1982). Cardinal directions of color space. *Vision Research, 22,* 1123–1131. [PubMed]

Krauskopf, J., & Zaidi, Q. (1986). Induced desensitization. *Vision Research, 26,* 759–762. [PubMed]

Lee, B. B., Martin, P. R., & Valberg, A. (1989). Nonlinear summation of m-cone and l-cone inputs to phasic retinal ganglion-cells of the macaque. *Journal of Neuroscience, 9,* 1433–1442. [PubMed] [Article]

Lee, J., & Stromeyer, C. F. (1989). Contribution of human short-wave cones to luminance and motion detection. *The Journal of Physiology, 413,* 563–593. [PubMed] [Article]

Lee, S. C. S., Telkes, I., & Grünert, U. (2005). S-cones do not contribute to the OFF-midget pathway in the retina of the marmoset, Callithrix jacchus. *European Journal of Neuroscience, 22,* 437–447. [PubMed]

MacLeod, D. I., & Boynton, R. M. (1979). Chromaticity diagram showing cone excitation by stimuli of equal luminance. *Journal of the Optical Society of America, 69,* 1183–1186. [PubMed]

McKeefry, D. J., Parry, N. R. A., & Murray, I. J. (2003). Simple reaction times in color space: The influence of chromaticity, contrast, and cone opponency. *Investigative Ophthalmology & Visual Science, 44,* 2267–2276. [PubMed] [Article]

McLellan, J. S., & Eskew, R. T. (2000). ON and OFFS-cone pathways have different long-wave cone inputs. *Vision Research, 40,* 2449–2465. [PubMed]

Mollon, J. D. (1980). Post-receptoral processes in colour vision. *Nature, 283,* 623–624. [PubMed]

Mollon, J. D., & Krauskopf, J. (1973). Reaction time as a measure of the temporal response properties of individual colour mechanisms. *Vision Research, 13,* 27–40. [PubMed]

Piéron, H. (1931). La sensation chromatique. Données sur la latence propre et l'établissement des sensations de couleur. *Année Psychology, 32,* 1–29.

Pokorny, J., Smithson, H., & Quinlan, J. (2004). Photo-stimulator allowing independent control of rods and the three cone types. *Visual Neuroscience, 21,* 263–267. [PubMed]

Rabin, J., Switkes, E., Crognale, M., Schneck, M. E., & Adams, A. J. (1994). Visual-evoked potentials in 3-dimensional color space—Correlates of spatiochromatic processing. *Vision Research, 34,* 2657–2671. [PubMed]

Robson, A. G., & Kulikowski, J. J. (1998). Objective specification of tritanopic confusion lines using visual evoked potentials. *Vision Research, 38,* 3499–3503. [PubMed]

Rodieck, R. W. (1991). Which cells code for color? In A. Valberg & B. B. Lee (Eds.), *From pigments to perception: Advances in understanding visual processes* (pp. 83–93). New York: Plenum Press.

Schnapf, J. L., Nunn, B. J., Meister, M., & Baylor, D. A. (1990). Visual transduction in cones of the monkey Macaca fascicularis. *The Journal of Physiology, 427,* 681–713. [PubMed] [Article]

Shapiro, A., Pokorny, J., & Smith, V. (1996). Cone-rod receptor spaces with illustrations that use CRT phosphor and light-emitting-diode spectra. *Journal of the Optical Society of America A, Optics, Image Science, and Vision, 13,* 2319–2328. [PubMed]

Sharpe, L. T., Stockman, A., Jagla, W., & Jägle, H. (2005). A luminous efficiency function, V*(lambda), for daylight adaptation. *Journal of Vision, 5*(11):3, 948–968, doi:10.1167/5.11.3, http://journalofvision.org/5/11/3/. [PubMed] [Article]

Shinomori, K., Spillmann, L., & Werner, J. S. (1999). S-cone signals to temporal OFF-channels: Asymmetrical connections to postreceptoral chromatic mechanisms. *Vision Research, 39,* 39–49. [PubMed]

Shinomori, K., & Werner, J. S. (2008). The impulse response of S-cone pathways in detection of increments and decrements. *Visual Neuroscience, 25,* 341–347. [PubMed] [Article]

Smithson, H. E., & Mollon, J. D. (2004). Is the S-opponent chromatic sub-system sluggish? *Vision Research, 44,* 2919–2929. [PubMed]

Spillmann, L. (1990). Wahrgenommene Bunttonunterschiede auf gegenläufigen Farbkreiseln. *Farbe und Design, 49/50,* 18–24.

Spillmann, L., & Neumeyer, C. (1984). Änderung der Farbwahrnehmung bei gegensinniger Abfolge der Farbtöne im Farbenkreis. In L. Spillmann & B. R. Wooten (Eds.), *Sensory experience, adaptation and perception: Festschrift for Ivo Kohler* (pp. 495–508). Hillsdale, NJ: Lawrence Erlbaum.

Stockman, A., Langendorfer, M., Smithson, H. E., & Sharpe, L. T. (2006). Human cone light adaptation: From behavioral measurements to molecular mechanisms. *Journal of Vision, 6*(11):5 1194–1213, doi:10.1167/6.11.5, http://journalofvision.org/6/11/5/. [PubMed] [Article]

Stockman, A., MacLeod, D. I. A., & DePriest, D. D. (1987). An inverted S-cone input to the luminance channel: Evidence for two processes in S-cone flicker detection. *Investigative of the Ophthalmology Visual Science, 28,* 92.

Stockman, A., & Sharpe, L. T. (2000). The spectral sensitivities of the middle- and long-wavelength-sensitive cones derived from measurements in observers of known genotype. *Vision Research, 40,* 1711–1737. [PubMed]

Stockman, A., Sharpe, L. T., & Fach, C. (1999). The spectral sensitivity of the human short-wavelength sensitive cones derived from thresholds and color matches. *Vision Research, 39,* 2901–2927. [PubMed]

Stromeyer, C. F., Eskew, R. T., Kronauer, R. E., & Spillmann, L. (1991). Temporal phase response of the short-wave cone signal for color and luminance. *Vision Research, 31,* 787–803. [PubMed]

Sun, H., Smithson, H. E., Zaidi, Q., & Lee, B. B. (2006a). Do magnocellular and parvocellular ganglion cells avoid short-wavelength cone input? *Visual Neuroscience, 23,* 441–446. [PubMed]

Sun, H., Smithson, H. E., Zaidi, Q., & Lee, B. B. (2006b). Specificity of cone inputs to macaque retinal ganglion cells. *Journal of Neurophysiology, 95,* 837–849. [PubMed] [Article]

Tailby, C., Solomon, S. G., & Lennie, P. (2008). Functional Asymmetries in visual pathways carrying S-Cone signals in macaque. *Journal of Neuroscience, 28,* 4078–4087. [PubMed] [Article]

Ueno, T., Pokorny, J., & Smith, V. C. (1985). Reaction-times to chromatic stimuli. *Vision Research, 25,* 1623–1627. [PubMed]

Valberg, A., Lee, B. B., & Tigwell, D. A. (1986). Neurons with strong inhibitory S-cone inputs in the macaque lateral geniculate nucleus. *Vision Research, 26,* 1061–1064. [PubMed]

Vassilev, A., Mihaylova, M. S., Racheva, K., Zlatkova, M., & Anderson, R. S. (2003). Spatial summation of S-cone ON and OFF signals: Effects of retinal eccentricity. *Vision Research, 43,* 2875–2884. [PubMed]

Wiesel, T. N., & Hubel, D. H. (1966). Spatial and chromatic interactions in lateral geniculate body of rhesus monkey. *Journal of Neurophysiology, 29,* 1115–1156. [PubMed]

Yeh, T., Lee, B. B., & Kremers, J. (1995). Temporal response of ganglion-cells of the macaque retina to cone-specific modulation. *Journal of the Optical Society of America A, Optics, Image Science, and Vision, 12,* 456–464. [PubMed]

Zaidi, Q., & Shapiro, A. G. (1993). Adaptive orthogonalization of opponent-color signals. *Biological Cybernetics, 69,* 415–428. [PubMed]